# Observation of helical traveling-wave convection in a liquid bridge

Kurt A. Muehlner, Michael F. Schatz,[a)] Valery Petrov,[b)] W. D. McCormick, J. B. Swift, and Harry L. Swinney[c)]
*Center for Nonlinear Dynamics and Department of Physics, The University of Texas at Austin, Austin, Texas 78712*

We use infrared imaging to visualize time-dependent flow in a liquid bridge (Prandtl number 35 and aspect ratio 1) with an imposed vertical temperature gradient. The primary instability leads from an axisymmetric time-independent state to helical traveling waves with an azimuthal wavenumber $m = 1$. A secondary instability introduces an additional traveling wave with $m = 2$. The structure and phase of the modes is determined from the infrared images. © *1997 American Institute of Physics.* [S1070-6631(97)01906-5]

One of the simplest examples of flow driven by temperature-induced surface tension gradients (thermocapillarity) is convection in a liquid bridge, which is formed by pinning a column of liquid between two solid boundaries (Fig. 1). Liquid bridge convection models hydrodynamic effects in the growth of crystalline materials in float-zones, where the appearance of time-dependent convective flow can induce undesired variation in the composition of processed crystals.[1] Increased understanding of liquid bridge convection should provide insight into surface-tension-driven flows in a variety of contexts, including the control of such flows, which was recently demonstrated for a remote unstable state in a liquid bridge by application of a nonlinear control algorithm.[2]

The structure of liquid bridge convection remains largely undetermined in experiments. Data from a recent experiment[3] were interpreted as indicating axial traveling waves with an azimuthal wavenumber $m = 0$ for the primary instability at most parameter values with Prandtl number $Pr \gg 1$. The same data were later re-interpreted[4] as indicating azimuthal standing waves with $m > 0$. The ambiguity arises because measurements of time-dependent convection in liquid bridges have largely been restricted to time series from a few local probes.

We obtain global information about the flow by imaging temperature fields in the infrared spectrum. Convection in the purified silicone oil[5] of our bridge is driven by a variation of surface tension $\sigma$ at the gas–liquid interface, induced by imposing a temperature difference $\Delta T$ between the solid boundaries (Fig. 1). A liquid nitrogen cooled camera (Amber Engineering Co. Model 5256 with a $256 \times 256$ element indium–antimonide staring array) collects light with wavelengths in a 0.08 $\mu$m band centered at 4.61 $\mu$m emitted from fluid within $\sim$ 1 mm (the silicone oil's extinction length) of the liquid's surface. Thus, the measured temperature field represents a weighted average of fluid temperatures near the fluid's free surface. The camera's field of view is centered at azimuthal angle $\theta = 0°$; two mirrors allow the camera to see the full circumference of the bridge. Different spatial locations are compared by means of time series of images recorded for three axial strips ($-0.5 \leqslant z \leqslant 0.5$), each about 3° wide, centered at $\theta = 0°$, $\theta = 108°$ and $\theta = 252°$ (Fig. 1). Additionally, we measure the local temperature 0.3 mm outside the free surface with a spherical thermistor of diameter 0.6 mm located at $z = 0$ and $\theta = 270°$.

The dimensionless parameter which characterizes the strength of the surface tension forces that drive the flow is the Marangoni number, $M \equiv |d\sigma/dT|(\Delta T)l/\rho \nu \kappa$ (the fluid properties are given in Ref. 5). For small $M$, the convection is time independent; the flow becomes time dependent with a single fundamental frequency at $M \approx 13000$ in our experiment. The onset of time dependence is sensitive to the fluid volume,[6] which is equal to $\pi r^2 l = 85$ mm$^3$.

The characteristic frequencies are determined from time series (see Fig. 2) obtained by vertically averaging from $z = -0.05$ to $z = 0.05$ in each of the three 3°-wide axial strips. Power spectra of the time series centered at $\theta = 0°$ show the characteristic frequencies of the flow [Figs. 3(a) and 3(b)]. The sequence of images is temporally filtered (filter width, 0.01 Hz) at each characteristic frequency. The temporally filtered, axially averaged strips are cross-correlated to determine phase differences. The azimuthal wavenumber of the mode corresponding to each frequency is the integer multiple of $2\pi$ that is equal to the sum of the phase differences. Space–time diagrams for each dominant mode are shown in Figs. 3(c) and 3(d). The diagrams characterize the global
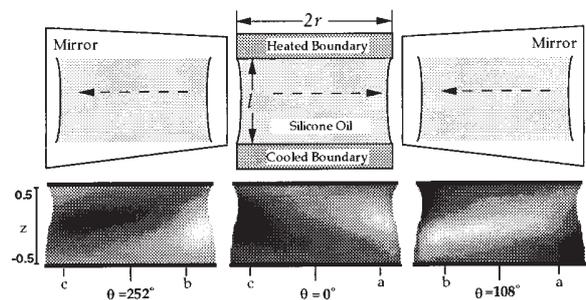


FIG. 1. Sketch (top figure) and images (bottom figures) of our liquid bridge convection experiment. The horizontal bridge boundaries are coaxial stainless steel cylinders with $r = 3.0$ mm and $l = 3.0$ mm. Simultaneous infrared images of the brightness temperature (darker shading for colder temperatures) are obtained for the full bridge circumference by use of mirrors. The helical structure of the temperature field corresponds to a traveling wave with azimuthal wavenumber $m = 1$. Note that the propagation direction for the two reflected images is opposite that of the center image, as indicated by dashed arrows in the sketch. Corresponding angles in the different images are indicated by the a, b and c (a < b < c).
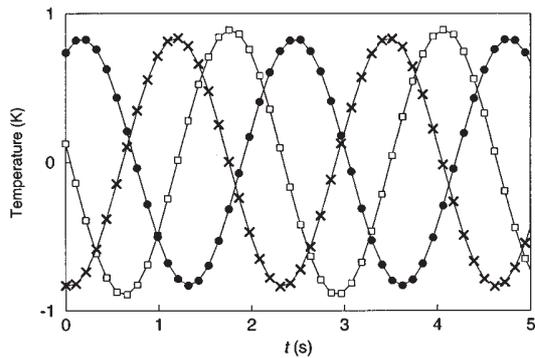
FIG. 2. Time series (averaged in $z$) of deviation from the mean temperature for time-periodic flow recorded in 3°-wide vertical strips at $\theta=0°$ ($\square$), $\theta=108°$ ($\bullet$) and $\theta=252°$ ($\times$) for $M=16300$.



FIG. 4. (a) The axial phase difference $\phi$ for the $m=1$ fundamental mode at $M=13400$($\bullet$), $M=16300$($\times$), and $M=19800$($\square$). (b) The axial phase difference $\phi$ for $m=2$ first harmonic at $M=16300$($\bullet$) and $M=19800$($\times$), and the $m=2$ mode arising from secondary instability at $M=19800$($\square$).

spatial structure of each traveling mode since periodicity in time and in azimuth ensures that the time dependence of each mode is equivalent to azimuthal spatial dependence. Thus, the images of an axial strip acquired during the time interval for a mode to propagate once around the bridge circumference [Figs. 3(c) and 3(d)] also represent the instantaneous spatial structure displayed for the full axial and azimuthal domain. These space–time diagrams exhibit a spatial structure matching that seen in direct images of the surface dynamics [compare Fig. 1 with Fig. 3(c)].

An $m=1$ traveling wave ($f_1=0.41$ Hz) is the fundamental mode just above the onset of time-dependent convection [Fig. 3(c)], and this mode has a harmonic with $m=2$ that travels with the same wave speed as the fundamental. Above the secondary instability an additional frequency arises, an

$m=2$ mode that is frequency locked to the fundamental; however, this mode propagates at 3/4 of the fundamental wavespeed [Fig.3(d)].

All the dominant modes arising from both the primary and secondary instability have a helical structure with isotherms at an oblique angle with respect to the $z$ axis. Figure 4 shows the axial phase dependence $\phi(z)$ obtained from cross-correlation between time series of different locations in an axial strip. The variation in phase for the $m=1$ fundamental mode is nearly linear with the same slope for various





FIG. 3. (a),(b) spectra and (c),(d) corresponding space–time diagrams, showing the dominant modes for states with a single fundamental frequency at (a) $M=16300$ and two fundamental frequencies at (b) $M=19800$. The space–time diagrams are constructed from narrow axial images at $\theta=0$. Images that are band pass filtered at the dominant frequencies show the spatio-temporal behavior of each mode, and the summation of these images shows the full surface dynamics. [The peak at 0.22 Hz in (b) is too weak to be visualized in (d).] The time interval for each mode to propagate through $\Delta\theta=360°$ is indicated above each diagram. To emphasize the connection to azimuthal spatial structure, time on the abscissa axis increases from right to left in (c) and (d).

FIG. 5. (a)Time series and (b)power spectra from a thermistor placed at $\theta = 270°$ and $z = 0$ at a distance 0.3 mm from the liquid surface, for a two-frequency state at $M = 19800$.

values of $M$, despite a change in amplitude by a factor of 10 and the onset of the secondary instability [Fig. 4(a)]. The $m = 2$ mode arising from the secondary instability has a similar monotonic variation in phase as the $m = 1$ mode; however, Fig. 4(b) shows that the $m = 2$ harmonic exhibits a local minimum and maximum in the axial phase variation.

Peaks at the subharmonic frequency ($\sim 0.2$ Hz) are much larger in power spectra of the local probe data [0.53 times the fundamental power, Fig. 5(b)] than in power spectra from infrared images [0.09 times the fundamental power, Fig. 3(b)]. Ratios of the other dominant peaks are similar for both sets of data, however, indicating that this effect is not due to decreasing probe frequency response. Thus, the thermistor time series may be mistakenly taken as evidence for a subharmonic (period-doubling) transition, whereas infrared imaging suggests the subharmonic arises from nonlinear interaction between the fundamental $m = 1$ mode and the secondary $m = 2$ mode. The enhanced subharmonic in the thermistor time series may be caused by the coupling between the gas and the liquid interface since the thermistor does not directly measure temperature in the liquid bridge.

Our infrared measurements provide an unambiguous determination of spatial structure that can be compared to theoretical computations and numerical simulations. For the time-periodic state, Rupp, Müller and Neumann[7] find an $m = 2$ traveling wave in a bridge of somewhat larger aspect ratio ($l/r = 2$) at $Pr = 49$; however, the onset of waves occurs at $M$ ($\approx 40000$), much larger than observed in experiment.[3] For $Pr = 35$, Xu and Davis[8] computed $m = 1$ helical traveling waves whose $z$ velocity component is oriented in the direction of the time-independent base flow, as in our experiment. However, no end effects were included in the $l \to \infty$ case Xu and Davis considered. Further calculations

at parameter values similar to our experiment are required to resolve these discrepancies, and to determine the nature of secondary instabilities, for which there are no theoretical predictions. Our method of infrared visualization should also enable determination of spatial structure for low Prandtl number ($\lesssim 1$) flows where more extensive theoretical work has been performed.[9–11]

[a]Present address: School of Physics, Georgia Institute of Technology, Atlanta, Georgia 30332. Electronic mail: mike.schatz@physics.gatech.edu

[b]Electronic mail: lera@chaos.ph.utexas.edu

[c]Electronic mail: swinney@chaos.ph.utexas.edu

[1] D. T. J. Hurle, W. Müller, and R. Nitsche, ''Crystal growth from the melt,'' in *Fluid Sciences and Materials Science in Space* (Springer, Berlin, 1987).

[2] V. Petrov, M. F. Schatz, K. A. Muehlner, S. J. VanHook, W. D. McCormick, J. B. Swift, and H. L. Swinney, ''Nonlinear control of remote unstable states in a liquid bridge convection experiment,'' Phys. Rev. Lett. **77**, 3779 (1996).

[3] R. Velten, D. Schwabe, and A. Scharmann, ''The periodic instability of thermocapillary convection in cylindrical liquid bridges,'' Phys. Fluids A **3**, 267 (1991).

[4] H. C. Kuhlmann and H. J. Rath, ''On the interpretation of phase measurements of oscillatory thermocapillary convection in liquid bridges,'' Phys. Fluids A **5**, 2117 (1993).

[5] The working fluid, tetradecamethylhexasiloxane [liquid density $\rho = 0.89$ g/cm$^3$, kinematic viscosity $\nu = 0.026$ cm$^2$/s, thermal diffusivity $\kappa = 0.000\,74$ cm$^2$/s and the surface tension temperature derivative $| d\sigma/dT | = 0.068$ dyne/(cm K) at 25 °C], is obtained with >95% purity using techniques described in M. F. Schatz and K. Howden, ''Purification of silicone oils for fluid experiments,'' Exp. Fluids **19**, 359 (1995).

[6] L. B. S. Sumner, G. P. Neitzel, P. Del Aversana, and J. P. Fontaine, ''The stability of thermocapillary convection in liquid bridges with highly deformed interfaces,'' Bull. Am. Phys. Soc. **39**, 1978 (1994).

[7] R. Rupp, G. Müller, and G. Neumann, ''Three-dimensional time dependent modelling of the Marangoni convection in zone melting configurations for GaAs,'' J. Cryst. Growth **97**, 34 (1989).

[8] J.-J. Xu and S. H. Davis, ''Convective thermocapillary instabilities in liquid bridges,'' Phys. Fluids **27**, 1102 (1984).

[9] G. P. Neitzel, K. T. Chang, D. F. Jankowski, and H. D. Mittelmann, ''Linear stability theory of thermocapillary convection in a model of the float-zone crystal-growth process,'' Phys. Fluids A **5**, 108 (1993).

[10] M. Wanschura, V. M. Shevtsova, H. C. Kuhlmann, and H. J. Rath, ''Convective instability mechanisms in thermocapillary liquid bridges,'' Phys. Fluids **7**, 912 (1995).

[11] M. Levenstam and G. Amberg, ''Hydrodynamical instabilities of thermocapillary flow in a half-zone,'' J. Fluid Mech. **297**, 357 (1995).